Subgrid粒子を含む気液二相流の直接シミュレーション

Direct simulation of gas-liquid two-phase flows with subgrid particles

○ 孫 明宇, 東北大学際センター, 仙台市青葉区荒巻字青葉, E-mail: sun@cir.tohoku.ac.jp
Mingyu Sun, Center for Interdisciplinary Research, Tohoku University, Sendai 980-8578, Japan

A new numerical model for the simulation of interfacial flows with subgrid-scale fluid structures is proposed. The model can handle two-phase phenomena with both resolved and subgrid length scales, for example, a large bubble of twenty grid spacing eventually shrinks to one-twentieth. The two-phase flows are modeled in two steps that treat two different length and time scales. The first Eulerian step deals with the length scale of the grid spacing and larger. This step is done by solving a hyperbolic system of equations, and numerically solved using an approximate Riemann solver. The second step, or the subgrid modeling, deals with the subgrid-scale interactions between two phases inside an interface cell. The subgrid modeling is equivalent to the relaxation procedure used in two-fluid models. An algebraic analytical solution has been found for the exchange of momentum, volume and energy to the second-order accuracy for both finite and instantaneous relaxations for materials with any EOS. The principle of maximum entropy is adopted to find a unique solution for energy exchanges. An interface with a high density ratio can be resolved sharply without producing non-physical oscillations. This paper focuses on the basic ideas of the method and 1-D tests.

1. Introduction

Interfacial phenomena with disparate or/and evolving length scales prevail in nature, such as bubble collapsing, fuel atomization, the breakup of water drops, the evolution of ocean waves, and volcano eruptions. A collapsing bubble may eventually reduce its original size to a minute fraction, which may be smaller than the grid spacing. For such a problem, the straightforward method is to use a grid fine enough to resolve all scales; however the computer time and storage required can be prohibitive, because the size and the location of the bubbles are hardly predictable. The motivation of this work is to develop a numerical technique for the volume-tracking method that can allow the existence of subgrid-scale fluid structures, and approximate them to reasonable accuracy, in addition to resolve large interfaces sharply as a sharp interface method.

Consider an interface with the length scale, d, say the diameter of a spherical particle, or equivalent diameter if non-spherical. Compared with the grid spacing that is restricted by computer resources, the length scales in two-phase phenomena can be generally divided to three scales, under-resolved ($d \ll \Delta x$), semi-resolved ($d = O(\Delta x)$) and resolved ($d \gg \Delta x$) scales. According to the length scale that can be best modeled, numerical methods developed for two-phase flows can be divided to two categories.

The sharp interface method can deal with flows containing particles sufficiently larger than the grid size. Popular methods under this category include the volume of fluid (VOF), the level-set, among many others. These methods can resolve the interface sharply, in one or two cells. The VOF method can be formulated conservatively, but the level-set is generally non-conservative. The treatment for subgrid particles is impossible by using up-to-date methods under this category. For the simulation of under-resolved particles, $d \ll \Delta x$, the diffuse interface methods (two-fluid models) are often used. These models assume a local mixture, distinguishing at least the volume fraction of two phases in a grid cell. Each phase is assumed to have own pressure and velocity or averaged/relaxed ones. This approximation allows strong numerical simplicity and eliminates the explicit treatment for interfaces. Depending upon the assumption adopted in such a model, the number of governing equations can vary from four to seven for 1-D flows. In practice, these models are supplemented by instantaneous relaxation or averaging procedures. This approach can simulate two-phase phenomena with any length scales, but an interface can only be resolved with a fairly wide stencil. An interface separating two pure fluids can never be resolved sharply as it should be.

This work tries to expand the capability of the traditional volume-tracking method to handle the fluid structure of semi-resolved scales, which has characteristics of both resolved and under-resolved length scales. The method for the tracking of subgrid scale particle has been reported [(1)], and this paper will focus on the model to evolve the solutions with subgrid scale fluid structures.

2. Modeling of two-phase flows with subgrid fluid structures

Consider a control volume or a cell consisting of two phases on a fixed Eulerian grid. It interacts with its neighboring volumes that are occupied by either one or two phases, and simultaneously the two phases inside interact with each other. The former represents the phenomena with length scales of the grid spacing and larger, and the latter represents those with subgrid scales. In this paper, we call the former external interaction, and the latter internal or subgrid interaction. The basic idea is to numerically model these two interactions in two steps that are solved by different methods, which are to be discussed in two following sections respectively.

2.1 Modeling of external interactions

The mathematical model for the external interactions consists of a hyperbolic system of eight equations. Suppose $\mathbf{U}_k$ represents the conservative quantities $\mathbf{U}_k = (\rho_k, \rho_k u_k, \rho_k E_k, 1)^T$, and α_k the volume fraction of phase k in the control volume, for the phase with a large volume m and the other phase s, the governing equations for the two phases are as follows,

$$(\alpha_s \mathbf{U}_s)_t + (\alpha_s \mathbf{U}_s u_m)_x = 0 \qquad (1)$$

and for the master phase with the large volume

$$(\alpha_m \mathbf{U}_m)_t + (\alpha_m \mathbf{U}_m u_m)_x = \mathbf{P}_x. \qquad (2)$$

The equations are solved by the first order Godunov-type scheme. The pressure and velocity at faces of control volumes are estimated from the HLLC approximate Riemann solver between two pure master phases, which are used to approximate the terms on the RHS. The

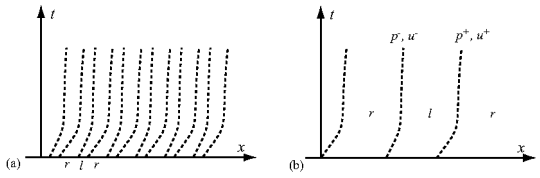

Fig. 1: Interface configurations inside the interface cell

volume fluxes of both fluxes can be calculated by either the exact location of the interface if the interface tracking method is used, or by the volume fraction in the upstream cell. The details and discussion of these treatments will be reported in a separate paper.

2.2 Modeling of subgrid interactions

The interactions between two phases are modeled in this section. Suppose there are N uniformly distributed phase pairs in the interface cell, as shown in Fig.1a, and every phase pair consists of two phases with the same quantities (density, pressure, velocity, temperature, volume fraction) as those defined in the cell.

The subgrid-scale interactions are modeled by two sets of conservation laws for two respective phases with interfaces between. In this work, the model is imposed with the periodic boundary condition, such that the resulting net flux is zero. Consider the left phase in a phase pair, as shown in Fig.1b, its solution is governed by both pressure and velocity at left and right boundaries, (p^-, u^-), (p^+, u^+) respectively. The conservation laws yield, at the discrete level for the left phase,

$$(M_l)_t = 0, \tag{3}$$

$$(M_l u_l)_t = N(p^- - p^+), \tag{4}$$

$$(M_l E_l)_t = N(p^- u^- - p^+ u^+), \tag{5}$$

$$(\Omega_l)_t = -N(u^- - u^+), \tag{6}$$

where M_l is the mass of the left fluid, satisfying

$$M_l = \rho_l \alpha_l \Delta x = \rho_l \Omega_l.$$

For the right phase, the conservation laws give

$$(M_r)_t = 0, \tag{7}$$

$$(M_r u_r)_t = -N(p^- - p^+), \tag{8}$$

$$(M_r E_r)_t = -N(p^- u^- - p^+ u^+), \tag{9}$$

$$(\Omega_r)_t = N(u^- - u^+). \tag{10}$$

We shall find an approximate solution to these equations without recoursing to iterations or local time stepping, satisfying following requirements.

(1) The solution at $t = \Delta t$ is at least second-order accurate, or the error is no more than $O(\Delta t^2, \Delta x^2)$;

(2) The solution is valid for $N \to +\infty$;

(3) The solution approaches the pressure and velocity equilibriums for $t \to +\infty$;

(4) The solution satisfies the entropy inequality.

2.2.1 Approximations Both velocities and pressures at faces are approximated by using the acoustic solver,

$$u^+ = \bar{u} + (p_l - p_r)/(\rho_l a_l + \rho_r a_r), \tag{11}$$

$$p^+ = \bar{p} + \bar{s}(u_l - u_r), \tag{12}$$

and

$$u^- = \bar{u} - (p_l - p_r)/(\rho_l a_l + \rho_r a_r), \tag{13}$$

$$p^- = \bar{p} - \bar{s}(u_l - u_r), \tag{14}$$

where

$$\bar{u} = (\rho_l a_l u_l + \rho_r a_r u_r)/(\rho_l a_l + \rho_r a_r),$$

$$\bar{p} = (\rho_l a_l p_r + \rho_r a_r p_l)/(\rho_l a_l + \rho_r a_r),$$

$$\bar{s} = (\rho_l a_l \rho_r a_r)/(\rho_l a_l + \rho_r a_r).$$

These approximations are valid before the fastest wave reaches the other side of the phase volume, or the system of equations should be integrated under the CFL condition if solved explicitly. It is prohibitive for very small particles. In order to overcome this stiffness, we consider a semi-implicit method, assuming that the phase quantities are time-dependent functions of $(p_l - p_r)$ and $(u_l - u_r)$ only. No other empirical assumptions are made in finding the solution to the equations.

The solution to the left phase equations is sufficient because of the conservation. It turns out that every equation in (4)-(6) can be integrated as an independent ODE under the above approximations. Momentum equation (4) is first solved in section 2.2.2, guaranteeing that the solution approaches the velocity equilibrium. Volume equation (6) is treated in section 2.2.3. In general, the volume exchange reduces the pressure difference. Special attention is paid to maintain the positivity of phase volumes. The energy equation (5) is solved based on two other solutions, and treated at last. The maximum entropy state in the possible solutions is pursued to remove the freedom in determining the energy flux.

2.2.2 Momentum exchange Consider the momentum equation for fluid l (4) in this section. Since no mass transfer between two fluids is considered, M_l remains constant, as seen from (3). The momentum equation is rewritten as

$$(u_l)_t = \frac{N}{M_l}(p^- - p^+).$$

Similarly for the right fluid one gets,

$$(u_r)_t = -\frac{N}{M_r}(p^- - p^+).$$

Subtracting the two velocities leads to

$$(u_l - u_r)_t = \frac{N}{\bar{M}}(p^- - p^+),$$

where

$$\bar{M} = (M_l M_r)/(M_l + M_r). \tag{15}$$

Approximating the two pressures by using the acoustic solver, $(p^- - p^+) = -2\bar{s}(u_l - u_r)$, gives

$$(u_l - u_r)_t = -\frac{2N\bar{s}}{\bar{M}}(u_l - u_r).$$

This ordinary differential equation yields

$$(u_l - u_r) = (u_l - u_r)_0 e^{-\frac{2N\bar{s}}{M}t}, \tag{16}$$

where $(u_l - u_r)_0$ denotes the initial velocity difference between two fluids. The subscript $_0$ is sometimes removed for the sake of clarity, the same for other initial values. A constant $\frac{N\bar{s}}{M}$ is assumed here. It is clear that the velocity difference will experience exponential decay with time. The resulting momentum change of the left fluid is,

$$\delta_{M_l u_l} = \int_0^t N(p^- - p^+)dt = -2N\bar{s}\int_0^t (u_l - u_r)dt. \tag{17}$$

Substituting (16) into (17) leads to the momentum change for left fluid,

$$\delta_{M_l u_l} = (u_l - u_r)_0 \bar{M}(e^{-\frac{2N\bar{s}}{M}t} - 1), \tag{18}$$

and for right fluid,

$$\delta_{M_r u_r} = -\delta_{M_l u_l}. \tag{19}$$

It can be readily seen that for $t \to +\infty$, the change of the momentum is finite, and the solution monotonely approaches the velocity equilibrium, as seen from (18). It is therefore valid not only in the early stage of interactions, but also provides a robust long-time solution.

Assuming a constant $\bar{s}$ introduces an error of $O(\Delta t)$, which introduces only an error of $O(\Delta t^2)$ in the momentum change. The same is held for volume and energy changes that follow.

2.2.3 Volume exchange The volume equation (6) will be integrated in this section. Consider the isentropic procedure,

$$\frac{dp_l}{d\Omega_l} = -\frac{M_l a_l^2}{\Omega_l^2}, \qquad \frac{dp_r}{d\Omega_r} = -\frac{M_r a_r^2}{\Omega_r^2}.$$

The pressure difference satisfies, since $\Omega_l + \Omega_r$ is a constant,

$$\frac{d(p_l - p_r)}{d\Omega_l} = -(\frac{M_l a_l^2}{\Omega_l^2} + \frac{M_r a_r^2}{\Omega_r^2}) = -(\frac{\rho_l a_l^2}{\Omega_l} + \frac{\rho_r a_r^2}{\Omega_r}) \equiv -\bar{c}. \tag{20}$$

Using (6), one gets

$$(p_l - p_r)_t = -N\bar{c}(u^- - u^+).$$

Approximating the velocity difference by the acoustic solver, $(u^- - u^+) = -\frac{2}{\rho_l a_l + \rho_r a_r}(p_l - p_r)$, yields

$$(p_l - p_r)_t = -\frac{2N\bar{c}}{\rho_l a_l + \rho_r a_r}(p_l - p_r).$$

The solution to this ODE is, if a constant coefficient is assumed,

$$(p_l - p_r) = (p_l - p_r)_0 e^{-\frac{2N\bar{c}}{\rho_l a_l + \rho_r a_r}t}, \tag{21}$$

where $(p_l - p_r)_0$ is the initial pressure difference. It is seen that the pressure difference approaches zero monotonely for $t, N \to +\infty$. The change of the pressure difference satisfies,

$$\delta_{(p_l - p_r)} = (p_l - p_r)_0 (e^{-\frac{2N\bar{c}}{\rho_l a_l + \rho_r a_r}t} - 1). \tag{22}$$

A simple way to evaluate the volume change of the left fluid is to integrate the pressure difference,

$$\delta_{\Omega_l} = -\int_0^t N(u^- - u^+)dt = \frac{2N}{\rho_l a_l + \rho_r a_r}\int_0^t (p_l - p_r)dt, \tag{23}$$

thus

$$\delta_{\Omega_l} = -\frac{\delta_{(p_l - p_r)}}{\bar{c}}. \tag{24}$$

which is consistent with (20). It is clear that the choice of $\bar{c}$ has a direct impact on the volume change. As seen from the definition of $\bar{c}$, it varies with the phase volume, and even approaches infinity for either phase volume being zero. In practice, the negative phase volume may appear when using a constant $\bar{c}$. Therefore assuming constant $\bar{c}$ is not appropriate for evaluating the volume change in numerical simulation.

We return to the original ODE (20), and integrate it directly,

$$(p_l - p_r) = \frac{M_l a_l^2}{\Omega_l} - \frac{M_r a_r^2}{\Omega - \Omega_l} + A_0, \tag{25}$$

where Ω_r has been replaced by $\Omega - \Omega_l$. Constant A_0 is determined from the initial state, $A_0 = (p_l - p_r)_0 - (\frac{M_l a_l^2}{\Omega_l} - \frac{M_r a_r^2}{\Omega_r})_0$. After simple algebraic calculations, we get a parabolic equation for Ω_l,

$$A_1\Omega_l^2 - (M_l a_l^2 + M_r a_r^2 + \Omega A_1)\Omega_l + \Omega M_l a_l^2 = 0, \tag{26}$$

where $A_1 = (p_l - p_r) - A_0$. As seen from (25), pressure difference $(p_l - p_r) \to +\infty$ for $\Omega_l \to 0$, and $(p_l - p_r) \to -\infty$ for $\Omega_l \to \Omega$. It is clear then that for any finite pressure difference $(p_l - p_r)$, a solution $\Omega_l \in (0, \Omega)$ exists. Thus, the positivity of volume is maintained for $t, N \to +\infty$.

Given a time t, pressure difference $(p_l - p_r)$ is obtained from (21). The left volume is one root of (26), and then the volume change is

$$\delta_{\Omega_l} = \Omega_l - (\Omega_l)_0. \tag{27}$$

2.2.4 Energy exchange Given momentum and volume changes, the energy change is evaluated by integrating (5),

$$\delta_{M_l E_l} = \int_0^t N(p^- u^- - p^+ u^+)dt,$$

which is further simplified to

$$\delta_{M_l E_l} = \hat{u}\int_0^t N(p_l^- - p_r^+)dt + \hat{p}\int_0^t N(u_l^- - u_r^+)dt, \tag{28}$$

or

$$\delta_{M_l E_l} = \hat{u}\delta_{M_l u_l} - \hat{p}\delta_{\Omega_l}, \tag{29}$$

where $\hat{u}$ is the value of $\bar{u}$ at $t' \in [0, t]$, and $\hat{p}$ is that of $\bar{p}$. Since both velocity and pressure are relaxed over time, it is nature to expect that they vary within the bounds

$$\hat{u} \in [u_l, u_r] \tag{30}$$

and

$$\hat{p} \in [p_l, p_r]. \tag{31}$$

We shall find a solution within the bounds (30) and (31) such that energy change $\delta_{M_l E_l}$ results in the state

of maximum entropy in the cell. Consider $\xi_1, \xi_2 \in [0,1]$, $\hat{u}$ and $\hat{p}$ satisfying (30) and (31) are expressed as

$$\hat{u} = u_l + \xi_1(u_r - u_l),$$

$$\hat{p} = p_l + \xi_2(p_r - p_l).$$

Substituting them into (29) gives

$$\delta_{M_l E_l} = u_l \delta_{M_l u_l} - p_l \delta_{\Omega_l} + \chi, \tag{32}$$

where

$$\chi = \xi_1(u_r - u_l)\delta_{M_l u_l} - \xi_2(p_r - p_l)\delta_{\Omega_l}.$$

By using the solutions for $\delta_{M_l u_l}$ and δ_{Ω_l},

$$(u_r - u_l)\delta_{M_l u_l} = (u_l - u_r)^2 \bar{M}(1 - e^{-\frac{2N\bar{s}}{M}t}) \geq 0,$$

$$-(p_r - p_l)\delta_{\Omega_l} = (p_r - p_l)^2(1 - e^{-\frac{2N\bar{c}}{\rho_l a_l + \rho_r a_r}t})/\bar{c} \geq 0,$$

it is clear that

$$\chi \in [0, \chi_{max}], \quad \chi_{max} = (u_r - u_l)\delta_{M_l u_l} - (p_r - p_l)\delta_{\Omega_l}. \tag{33}$$

Now, two parameters, $\hat{u}$ and $\hat{p}$, have been reduced to one parameter χ. In what follows, we shall find χ such that the resulting state in the cell attains the maximum entropy under the constraint $\chi \in [0, \chi_{max}]$.

Consider the cell consisting of two interacting phases. The cell is regarded as an isolated thermodynamic system because of the periodic condition. The entropy inequality requests that the total entropy of two phases is not decreased after the subgrid modeling. Because the energy change (32) includes all possible solutions resulted from volume and momentum changes in the subgrid modeling, it is no need to consider intermediate processes, such as the volume compression/expansion in pressure relaxation. The construction of the maximum entropy for the final state is sufficient, and it is also more efficient than treating those changes separately. Only the process of energy exchange under the constant volume is considered.

The entropy change should attain the extreme point, thus χ satisfies

$$\frac{d\delta_S}{d\chi} = \frac{d\delta_{Sl}}{d\chi} + \frac{d\delta_{Sr}}{d\chi} = 0, \tag{34}$$

where δ_{Sl} and δ_{Sr} are the entropy change of left and right phases after energy exchange.

First, we evaluate $\frac{d\delta_{Sl}}{d\chi}$. The change of internal energy follows, for the left phase,

$$\begin{aligned} \delta_{M_l e_l} &= \tfrac{1}{2}M_l u_l^2 + (u_l \delta_{M_l u_l} - p_l \delta_{\Omega_l} + \chi) \\ &\quad - \tfrac{1}{2}M_l(u_l + \tfrac{\delta_{M_l u_l}}{M_l})^2 \\ &= \chi - (p_l \delta_{\Omega_l} + \tfrac{\delta_{M_l u_l}^2}{2M_l}) \\ &\equiv \chi - B_l, \end{aligned} \tag{35}$$

where $B_l = p_l \delta_{\Omega_l} + \frac{\delta_{M_l u_l}^2}{2M_l}$. The entropy change is then

$$\begin{aligned} \delta_{Sl} &= \int_0^{\delta_{M_l e_l}} \tfrac{1}{T_l} de \\ &= \int_0^{\delta_{M_l e_l}} [\tfrac{1}{T_{l0} + e/C_{vl}} + O(\delta^2)] de \\ &= \int_0^{\delta_{M_l e_l}} \tfrac{C_{vl}}{C_{vl}T_{l0} + e} de + O(\delta^3), \end{aligned} \tag{36}$$

where $C_{vl} = (\partial e/\partial T)_v$ is the heat capacity of the left phase under constant volume. The temperature appearing in the denominator has been linearized. Its change with χ satisfies

$$\frac{d\delta_{Sl}}{d\chi} = \frac{C_{vl}}{C_{vl}T_{l0} + \delta_{M_l e_l}} \frac{d\delta_{M_l e_l}}{d\chi} = \frac{C_{vl}}{C_{vl}T_{l0} + \chi - B_l} \tag{37}$$

Similarly the right phase yields

$$\frac{d\delta_{Sr}}{d\chi} = -\frac{C_{vr}}{C_{vr}T_{r0} - \chi + B_r}, \tag{38}$$

where $B_r = p_l \delta_{\Omega_l} - \frac{\delta_{M_l u_l}^2}{2M_r} + (u_r - u_l)\delta_{M_l u_l}$.

Substituting (37) and (38) into (34), after a few algebraic manipulations, one gets

$$\chi = \frac{(C_{vr}T_{r0} + B_r)C_{vl} - (C_{vl}T_{l0} - B_l)C_{vr}}{C_{vl} + C_{vr}}, \tag{39}$$

which corresponds to the maximum point since

$$\frac{d^2\delta_S}{d\chi^2} = -[\frac{C_{vl}}{(C_{vl}T_{l0} + \chi - B_l)^2} + \frac{C_{vr}}{(C_{vr}T_{r0} - \chi + B_r)^2}] < 0.$$

Thus, the energy flux (32) is uniquely determined.

The maximum entropy guarantees the positivity of temperature in principle. Numerically, for materials with a constant heat capacity (e.g., perfect gases), the linearization for temperature adopted in (36) is exact, so that the positivity of temperature is always preserved.

It is noted that the state of maximum entropy adopted here does not lead to the temperature equilibrium in the interface cells in general. The energy exchange is constrained by (32), which is nonzero only for mechanical non-equilibrium flows. An interface with a temperature difference in the equilibriums will not be affected.

This completes all solutions required for the subgrid modeling.

3. Numerical tests

3.1 Preliminaries

Numerical model and techniques proposed in previous sections do not rely on the choice of the equation of state (EOS). In order to verify the methodology developed, the calorically perfect gas and water are tested, and their EOS and sound speed are summarized as following. The EOS of the perfect gas is given by

$$p = (\gamma - 1)\rho e, \tag{40}$$

and the sound speed by

$$c = \sqrt{\gamma p/\rho}, \tag{41}$$

where γ is the ratio of specific heats, which is 1.4 for diatomic gases and 1.66 for monoatomic gases.

The water is assumed to follow the Tait equation,

$$p = B[(\rho/\rho_c)^n - 1] + A, \tag{42}$$

where A, B and n are constants, $A = 10^5 Pa$, $B = 3.31 \times 10^8 Pa$ and $n = 7.15$. ρ_c is the density of water under pressure A, taken as $10^3 kg/m^3$. The Tait equation is fitted for experimental data at high pressure and density. The sound speed can be derived from the Tait equation,

$$c^2 = (nB/\rho_c^n)\rho^{n-1}. \tag{43}$$

The internal energy follows

$$e = c_v T + \frac{B\rho^{n-1}}{(n-1)\rho_c^n} + \frac{B-A}{\rho}, \qquad (44)$$

where c_v is the heat capacity of water, $4.2kJ/kg/K$, and T is the temperature.

All data without units are non-dimensionalized by characteristic quantities, $1m$ for length, 10^5Pa for pressure, $293.0K$ for temperature, $\sqrt{RT} = 49.36m/s$ for velocity, and $20.2ms$ for time. The numerical solutions are found in the spatial domain $0 \leq x \leq 1$ generally using 100 cells. The Courant number is always taken as 0.8. For each test problem, an initial location of discontinuity, x_0, and the output time are selected; these are stated in the caption of each figure. For comparison, a numerical solution obtained using ten thousand cells are plotted as solid lines representing the exact solutions. Note that there are two values of each primitive quantity in the interface cell in general. Both values are plotted, and placed at the reconstructed interface location.

3.2 Interface in a shock-tube problem

An air-helium shock tube problem, containing only one interface, is tested. The interface is resolved by a 1-D VOF tracking method. Initial conditions on left and right sides are listed in the table. In this case, the interface moves at a constant speed without interacting with ambient flows, except the very early stage immediately after diaphragm rupture.

Tab. 1: Data for the first test for resolved-interfaces

$(\rho, u, p, \alpha_{\text{air}})^L$	air (1.0, 0.0, 1.0, 1.0)
$(\rho, u, p, \alpha_{\text{air}})^R$	helium (0.125, 0.0, 0.1,0.0)

This problem has been tested by various resolved volume methods. The solution consists of a right traveling shock, an interface, and left expansion waves, as shown in Fig. 2a. The flow is subsonic on both sides of the interface. Velocity and pressure near the interface are resolved smoothly without generating spurious oscillations, and agree well with the exact solution. These pressure and velocity results are not shown in the paper. The volume tracking approach resolves the interface sharply for all N without any numerical fix. The influence of the number of interfaces is hardly visible even in the magnified scale as shown in Fig. 2a. It suggests the number of interfaces in the subgrid modeling, N, has little effect on the interface that is not far from the mechanical equilibriums as expected. This is the case for most particles that are sufficiently larger than the grid spacing.

3.3 Problem of bubble collapsing

The bubble collapse is modeled as a high speed water jet impinging on another stationary water column with an air cavity between. The $x-t$ diagram of this phenomenon is shown in Fig. 3. The water jet of $u = 40$ $(1.97km/s)$ with its surface initially located at $x = 0.4$, moves from left to right, and the stationary water column locates its surface at $x = 0.6$. Their surfaces are denoted as left and right interfaces in the figure. A 0.2 wide air cavity bubble is formed between these two interfaces. Initially, the velocity of the air bubble is set to be zero, and the initial pressure for all phases are 1 (10^5Pa). If the deceleration due to air drag was neglected, the water jet would impact on the water column

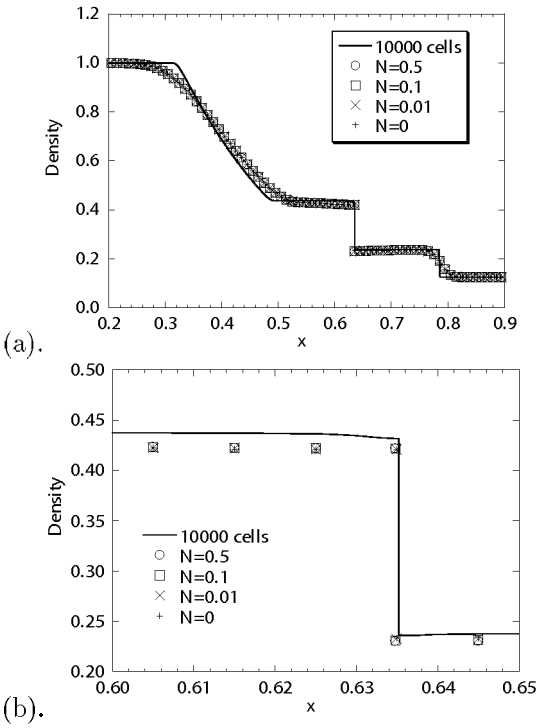

Fig. 2: Solutions of an interface in a shock-tube problem between helium and air for various N, $x_0 = 0.5$, $t = 0.15$: a) density distribution pressure; (b) magnified view of (a) near the interface.

at $t = 0.005$, an important time to estimate the size of the bubble. The air cavity shrinks with the compression of the left interface that moves almost at a constant speed before the impact. After the impact, the jet and the water column attain an equilibrium speed of 20, a half of the initial jet speed. The bubble cavity eventually reduces to $d = 4.8 \times 10^{-4}$, 0.24% of its initial size at $t = 0.006$. This simple but challenging case is designed for accessing the capability of a numerical method for two-phase flows with a wide range of length scales. It is very tough for all two phase methods.

The solution at the very early stage is plotted in Fig. 4a. It is clear that the pressures in the interface cell are only slightly affected by the N parameter in the subgrid modeling after the sudden impact of the water column. In what follows, N is set to be 0.5.

Solutions at three typical stations before, at and after the jet impact are investigated, and results are shown in Figs. 4b-d. The size of the collapsing bubble is about $2cm$, $0.17cm$ and $0.048cm$ respectively. A fixed grid number of 100 cells is used, and the grid size is thus $1cm$. The smallest bubble is just about $\Delta x/20$. Non-conservative methods are expected to lose the bubble eventually.

The supersonic jet interacts with the air bubble first, and creates two shock waves. One travels to the left in water, the left-most shock in Fig. 4b, and the other propagates in air. The shock in air hits the water column first, creating one reflected shock in the bubble and one transmitting shock in the water column. It is seen that there are three shock waves in Fig. 4b. Two shock waves in water are widely spread mainly due to the stiffness of Tait EOS and the first-order discretization. The volume-tracking method resolves well

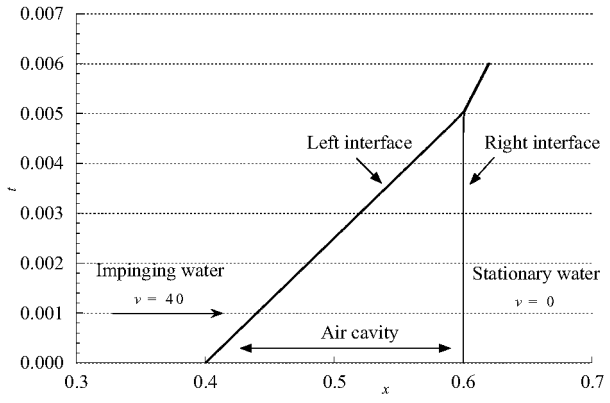

Fig. 3: Test of bubble collapse: a water jet of $v = 40$ $(1.97km/s)$ impacting on a stationary water column with a $0.2m$ wide air cavity between. The bubble cavity eventually reduces to $d = 0.48mm$ at $t = 0.006$ $(121\mu s)$.

the large-scale phenomena, such as the pressure behind the reflected shock wave in water.

The shock wave reflected from the right interface meets the coming left interface, and reflects again. The shock wave repeatedly reflects inside the air bubble. Fig. 4c is exactly the instant these reflections prevail, a truly non-equilibrium flow. The bubble has reduced to one fifth of the grid size. There are two pressures in the interface cells. Notice that although the bubble is smaller than the grid spacing, it lies on a grid line, so that there are two interface cells.

Fig. 4d shows the results when the bubble has attained the equilibrium state. Pressure and velocity results agree excellently well with those of the fine grid solutions. It is seen even for such a small bubble, the volume-tracking can resolve the density and temperature reasonably well. We emphasize that this accuracy is achieved by using a grid twenty times as large as the bubble after numerous shock interactions.

4. Concluding remarks

The proposed method is also amendable to two and three dimensions on any structured and unstructured grids by using the finite volume method. The extension to multi-dimensions can be straightforwardly done for the two-fluid model. The only difficulty for the resolved-volume approach in high dimensions is how to track and evolve a subgrid particle [(1)]. The onset of defragmentation in shock-water column interaction has been successfully investigated [(2)].

The present model is numerically simple, and physically valid for equilibrium flows, and non-equilibrium bubbly flows. The model does not assume the velocity slip at volume faces, which remains questionable for strongly non-equilibrium dusty flows.

Reference

(1) M. Sun, Volume-tracking of subgrid particles, Intl J. for Num. Methods in Fluids, (2010) DOI: 10.1002/fld.2331

(2) Igra D, Sun M Shock-water column interaction, from initial impact to fragmentation onset, AIAA J. (2010) DOI: 10.2514/1.44901.

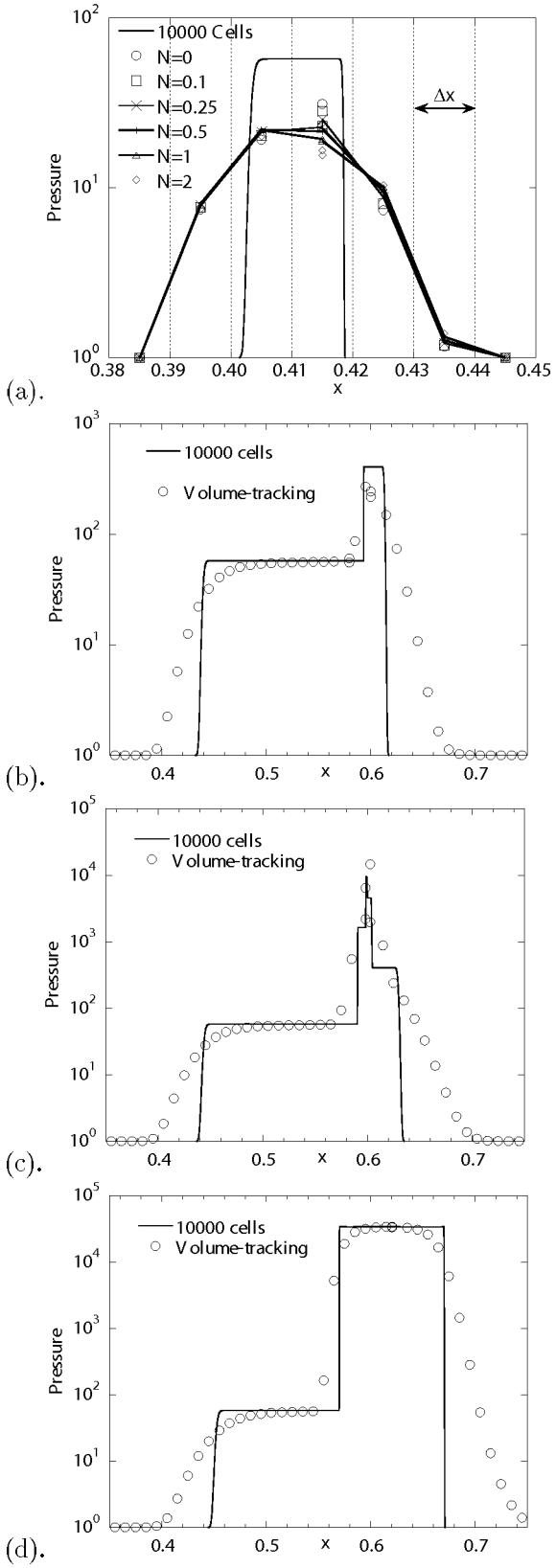

Fig. 4: Test of bubble collapsing: (a) very early stage for the left interface has travel a distance of $1.5\Delta x$ at $t = 0.000375$, (b)$t = 0.0045$; (c) $t = 0.005$; (d) $t = 0.006$